Author(s): Saloriutta, Karri & Uppstu, Andreas & Harju, Ari & Puska, Martti J.

Title: Ab initio transport fingerprints for resonant scattering in graphene

Year: 2012

Version: Final published version

Please cite the original version:

Saloriutta, Karri & Uppstu, Andreas & Harju, Ari & Puska, Martti J.. 2012. Ab initio transport fingerprints for resonant scattering in graphene. Physical Review B. Volume 86, Issue 23. 235417/1-7. 1550-235X (electronic). DOI: 10.1103/physrevb.86.235417.

Ab initio transport fingerprints for resonant scattering in graphene

Karri Saloriutta,[1,*] Andreas Uppstu,[2] Ari Harju,[2] and Martti J. Puska[1]

[1]*COMP Centre of Excellence, Department of Applied Physics, Aalto University School of Science, P.O. Box 11100, FIN-00076 AALTO, Finland*

[2]*COMP Centre of Excellence and Helsinki Institute of Physics, Department of Applied Physics, Aalto University School of Science, P.O. Box 14100, FIN-00076 AALTO, Finland*

(Received 28 August 2012; published 12 December 2012)

We have recently shown that by using a scaling approach for randomly distributed topological defects in graphene, reliable estimates for transmission properties of macroscopic samples can be calculated based even on single-defect calculations [A. Uppstu *et al.*, Phys. Rev. B **85**, 041401 (2012)]. We now extend this approach of energy-dependent scattering cross sections to the case of adsorbates on graphene by studying hydrogen and carbon adatoms as well as epoxide and hydroxyl groups. We show that a qualitative understanding of resonant scattering can be gained through density functional theory results for a single-defect system, providing a transmission "fingerprint" characterizing each adsorbate type. This information can be used to reliably predict the elastic mean free path for moderate defect densities directly using *ab initio* methods. We present tight-binding parameters for carbon and epoxide adsorbates, obtained to match the density-functional theory based scattering cross sections.

DOI: 10.1103/PhysRevB.86.235417 PACS number(s): 73.22.Pr, 71.15.Mb

I. INTRODUCTION

Electron transport in graphene has been studied widely from different angles due to its fundamental and application-derived importance (for reviews, see Refs. 1 and 2). Depending on the nature of the graphene sample and the substrate on which transport is measured, different scattering mechanisms have been proposed. For graphene on SiO_2, scattering from charges in the substrate is believed to be an important contribution.[3,4] On the other hand, resonant scattering from impurities, such as adsorbates and defects, can be large on a high-κ substrate and depend on the way the sample has been synthesized and cleaned.[5,6] We concentrate here on this latter case of resonant scattering. In addition to its importance for understanding the fundamental properties of experimental samples, which are seldom fully without adsorbed species, understanding resonant scattering might be relevant for the purposeful modification of graphene properties through functionalization.

Resonant scattering in graphene nanostructures is often studied numerically by a tight-binding model (TB) so that numerous calculations are performed for samples containing a set number of randomly placed defects. The results are then averaged in order to obtain for every defect concentration defect-specific properties, such as the elastic mean free path or the conductance, as a function of the charge carrier energy. This kind of ensemble averaging is a costly procedure even in the lightweight TB picture of the electronic structure. Therefore, based on prior work on electron transmission in silicon nanowires,[7,8] we have recently applied the concept of energy-dependent scattering cross section to scale the transport properties of single defects to those of macroscopic samples with homogeneous defect concentrations.[9]

The TB calculations can be parametrized based on the density functional theory (DFT) results or empirically based on experimental data. However, the modeling of defects beyond simple alterations in the topology, that is, the modeling of impurities, chemical adsorbates, or even carbon adatoms that create different bond configurations, becomes challenging since the parametrization should catch all the features of the chemical bonds relevant for the transport properties. A systematic determination of an adequate TB model is thus difficult and there are competing parametrization even for simple cases such as hydrogen.[10,11] Therefore, in this work we study the determination of the effective scattering cross sections directly from the DFT results for systems containing only a single defect. We also show that the single defect scattering cross section can be used to determine the optimal TB model parameters for transport calculations. In this way we fit the TB parameters using a quantity directly related to the resonant electron scattering by the defect in question.

First, we study hydrogen atoms and hydroxyl groups which are adsorbed on top of a carbon atom. The hydrogen atom is a good test case because there are different TB models to describe it and we can compare results given by them with DFT results. The adsorption of the hydroxyl group increases the complexity from that of the hydrogen atom and the DFT results for the scattering cross section show clear deviation from the hydrogen case. Oxygen is adsorbed in the form of epoxide on the carbon-carbon bridge which also increases the complexity of the chemical bonding. We compare the DFT results with those of a recent TB parametrization[12,13] and find out that the scattering cross sections from these two methods match apart from some details in regions of rapid variations. We show that these details can be improved by optimizing the TB parameters.

Furthermore, we present a TB model for a carbon adatom bound to the carbon-carbon bridge. The parameters are obtained by optimizing the TB scattering cross section to match the corresponding DFT prediction.

All the adsorbates we study are important from the experimental point of view and have potential for technological applications. Hydrogen is an important functionalizer that turns graphene into *graphane*, a band insulator, at full coverage.[14,15] At lower coverage, evidence for metal-insulator transition has been seen.[16] Oxygen can break graphene sheets or unzip carbon nanotubes to GNRs.[17,18] Epoxide is also a component of graphene oxide,[19,20] which has been used

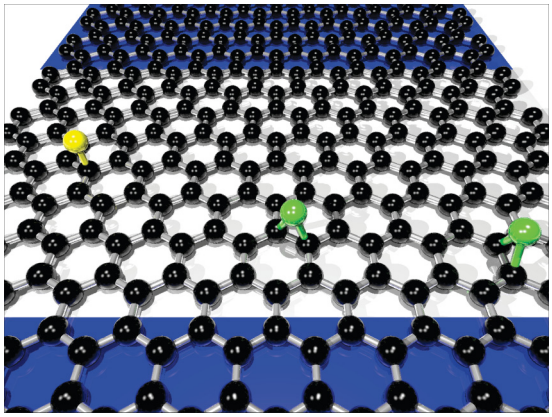

FIG. 1. (Color online) Two-probe transport geometry consisting of two ideal leads and a central scattering region. The graphene sheet is oriented with the transport along the armchair direction. Upper and lower shadowed (blue/gray) regions indicate the leads. The leftmost adsorbate on the scattering region is on top of a carbon atom and the others show two of the three bridge positions with different orientations with respect to the current.

for graphene synthesis[21] and sensor applications.[11,22] Carbon adatoms, on the other hand, are created during irradiation of graphene, for example, when intentionally creating vacancy and bond rotation defects.[23]

The organization of the paper is as follows. In Sec. II we describe the electronic structure models and methods used and review the main ideas for the the scattering cross section concept. In Sec. III we study the effect of different approximations on the scattering cross section for the atop-adsorbed hydrogen and hydroxyl as test cases. In Sec. IV we concentrate on the effect of the adsorbate chemistry by presenting results for oxygen and adatom carbon preferring bridge-site adsorption.

II. METHOD

Figure 1 shows the schematic setup for a two-probe transport calculation. The current flows between the shaded leads. The graphene sheet is oriented so that the armchair edge is parallel to the transport direction. The ribbons we study are thus armchair graphene nanoribbons (AGNRs), and we restrict our DFT calculations to shown ribbons with 23 carbon dimer lines (23-AGNRs).

The transmission through the ribbon or sheet is affected by the scattering of electrons off adsorbates and studied by the "standard" setup for *ab initio* transport calculations, that is, the combination of DFT and nonequilibrium Green's functions (NEGFs).[24] We use the TRANSIESTA implementation, a part of the SIESTA DFT package.[25,26]

We compare the full *ab initio* approach with the widely used nearest-neighbor TB model of graphene. The TB approach is based on the Hamiltonian

$$H = \sum_{\langle i,j \rangle} t c_i^\dagger c_j + \text{H.c.}, \tag{1}$$

where the sum is taken over the nearest neighbor pairs and the nearest neighbor hopping element t is -2.7 eV. An ideal (unrelaxed) vacancy can be described simply by removing the hopping elements to a particular carbon site. This is also the simplest model for a hydrogen adatom on top of a carbon atom since it describes the removal of the carbon π bond due to the creation of a carbon-hydrogen bond.

In order to more realistically describe an adatom on top of a carbon atom, the simple TB model can be complemented by an Anderson impurity level added to the Hamiltonian in (1), that is,

$$H = \sum_{\langle i,j \rangle} (t c_i^\dagger c_j + t c_j^\dagger c_i) + e_A d^\dagger d + t_A d^\dagger c_m + t_A c_m^\dagger d, \tag{2}$$

where the carbon atom with the index m is coupled with hopping t_A to the impurity level with energy e_A. This simple and versatile model has been widely used to model hydrogen and various other adsorbates, such as the hydroxyl group and hydrocarbons, that bind on top of a carbon atom.[10,11,27] For hydrogen, the parameters giving results corresponding well to DFT calculations[10] are $t_A = -2t$ and $e_A = t/16$ though other values have also been proposed.[11]

In our DFT calculations we use the double ζ polarization (DZP) basis set for relaxing the structures with the Broyden algorithm so that ionic forces are less than 0.04 eV/Å. We use the PBE functional for exchange and correlation.[28] The basis set is automatically constructed by SIESTA based on an energy shift of 80 meV and a split norm of 0.3 for all elements apart from hydrogen for which 0.5 is used. The grid interval corresponding to the Fourier cutoff energy of 250 Ry is used for the real-space grid. The periodic images are separated by 19 Å of vacuum. These parameters lead to a graphene lattice constant of 1.43 Å which is used in all the calculations. For transport the basis set is decreased to the single ζ polarization (SZP) and the grid to 150 Ry.

In addition to nanoribbons, we study the transmission through periodic systems, that is, graphene sheets. The sheets are oriented so that the transport is along the armchair direction. The system sizes are chosen so that the scattering cross section defined below is well-converged requiring the supercells to correspond to nanoribbons from 24-AGNRs to 32-AGNRs depending on the adsorbate studied. The periodicity is handled by a Monkhorst-Pack k-point sampling perpendicular to the current direction, with 3 to 6 k points used for relaxation and 21 to 45 for transport.

Following Refs. 8 and 9, we define the scattering cross section:

$$\sigma(\omega) = W \frac{T_0(\omega) - \langle T(\omega) \rangle}{\langle T(\omega) \rangle}, \tag{3}$$

where W is the lateral width of the supercell for periodic graphene or the width of the nanoribbon for GNRs. $T_0(\omega)$ is the transmission through the pristine system without a defect and $\langle T(\omega) \rangle$ is the transmission through the defect averaged over the defect locations and orientations. The scattering cross section is a rather abstract quantity. Based on it we can however produce estimates for the transmission through a defective sample with some finite defect density. For a sample of length L with different defect species with scattering cross sections σ_i and densities n_i we get

$$\langle T(\omega) \rangle = \frac{T_0(\omega)}{1 + L \sum_i n_i \sigma_i(\omega)}, \tag{4}$$

within the Ohmic regime. We can also estimate quantities that can be directly experimentally measured. The elastic mean free path, for example, is given by

$$l_e(\omega) = \sum_i \frac{1}{n_i \sigma_i(\omega)}. \quad (5)$$

Both Eqs. (3) and (4) are defined within the Ohmic regime where the transmissions can be averaged directly as the transmission has a Gaussian probability distribution. The cross section can, however, also be defined within the localized regime, as was done in our previous work.[9] This is seldom needed for cross sections based on single defect calculations and we concentrate on the Ohmic regime here.

One weakness of using the scaling approach in this manner is that we are assuming a random distribution of absorbents on graphene. If this is not the case and the disorder is *correlated*, the approach loses some of its validity. Indeed, there are indications that oxygen adsorbates, for example, tend to favor clustering since this is preferred energetically.[20] Correlation between *Coulombic* scatterers, on the other hand, can be used to explain the transport properties of graphene samples with no resonant scattering.[29]

DFT can be used to study spin-polarized transport and thus could be used to calculate a spin-dependent scattering cross section. All our calculations, however, are done spin compensated despite the fact that some of the systems we study in fact have a finite magnetic moment in the ground state. The addition of spin dependence would make the analysis of disordered systems much more complicated since long-range ordering of the spins is likely.[30,31] We also consider just armchair ribbons since zigzag ribbons have spin-polarized edges. Adding spin polarization to the calculations would split the resonance peaks at the Fermi energy into two closely spaced spin-polarized peaks.[32] The scattering cross section for the both spin channels would then be very similar to the spin-compensated cross sections presented here.

III. ATOP ADSORBATES: THE ATOMIC HYDROGEN AND HYDROXYL GROUP

To test the sensitivity of determining the adsorbate scattering cross sections on electronic-structure models and nanoribbon or bulk graphene geometries used, we first consider perhaps the simplest conceivable case, the hydrogen atom. This system is convenient since, as shown below, the TB model is enough to capture all the relevant physics with limited computational resources and even very large system sizes directly relevant to experiments can be studied.

As discussed above, the simplest TB model for hydrogen on graphene treats it as a vacancy. This is actually quite a poor model for a real vacancy since it does not account for the relaxation caused by the reorganization of the dangling bonds.[23] Figure 2(a) shows the electron transmissions for a pristine 23-AGNR and for a 23-AGNR with an adsorbed hydrogen in three different locations calculated with the vacancy TB model. Two of the three latter transmissions are very similar, with a dip right in the middle of the first transmission plateau at the Fermi energy while for one adsorbate location there is no dip. This is a general feature for metallic armchair nanoribbons: When hydrogen is adsorbed on a dimer indexable by 3N,

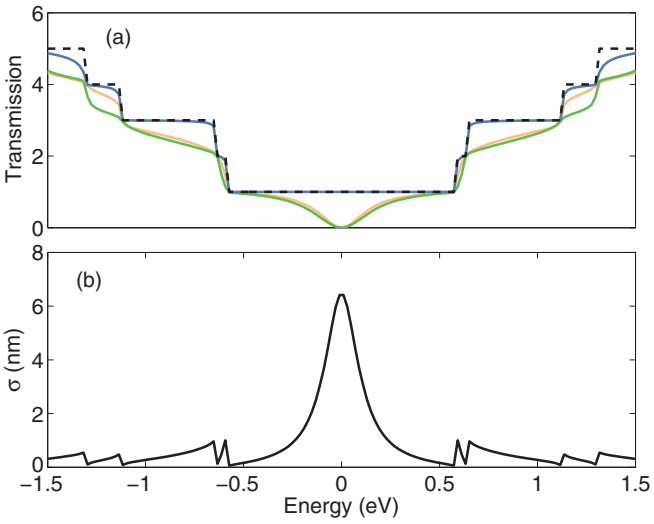

FIG. 2. (Color online) (a) Ideal electron transmission for a pristine 23-AGNR (dashed line) and transmissions for a 23-AGNR with one hydrogen atom adsorbed on three different locations (solid lines). (b) Scattering cross sections calculated by averaging over all the different adsorbate locations across the ribbon. The vacancy TB model is used. Here and in all the figures below, the Fermi energy is taken to be zero.

backscattering is suppressed due to the electronic structure of the ribbon.[33,34] Therefore the results for AGNRs shown below are calculated with Eq. (3) by averaging over all different adsorption sites. As an example of this, Fig. 2(b) shows the scattering cross section for the hydrogen adsorbate. The clearest feature is the strong peak at the Fermi energy that is caused by a resonant level at that energy and also shows up in the density of states. The other characteristic feature is the spikes further away from the Fermi level. They are due to the density of states van Hove singularities caused by the band edges of the quasi-one-dimensional system.

Ideally we would like to go from the scattering cross section of a narrow ribbon calculated using a full DFT approach by scaling to wider and longer systems using Eq. (4). Unfortunately, the details of the scattering cross section depend on the width of the nanoribbon. This is shown in Fig. 3(a) for the case of a hydrogen atom adsorbed on AGNRs of different width. The vacancy-model TB results indicate that the actual positions of the van Hove peaks depend on the ribbon width and that the central peak becomes thinner and higher as the ribbon width increases. It is however clear that it is possible to get a good qualitative understanding of the transmission for wider ribbons based on the scattering cross section calculated for a narrow ribbon.

Figure 3(b) shows the use of Eq. (4) by comparing an estimate based on the scattering cross section from a single defect calculation to an averaged transmission through a 100 nm long 125-AGNR. As long as the transmission is large enough, a very good estimate for the transmission through the longer sample can be generated. Close to the Fermi energy, the transmission is within the localized regime and the estimate based on Ohmic transmission [Eq. (4)] is larger than the average. Although here we concentrate on the Ohmic regime,

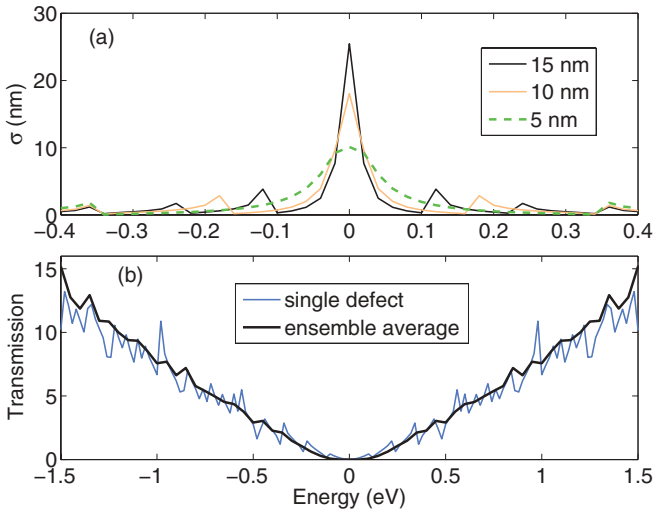

FIG. 3. (Color online) (a) Scattering cross sections for a hydrogen atom on AGNRs with different widths. The vacancy TB model is used. (b) Transmission through a 100 nm long 125-AGNR with 0.1% vacancy defect density. Comparison between results obtained by averaging over an ensemble of 50 samples with random defect locations (thick line) and an estimate from a single defect scattering cross section calculation (thin line). Notice the different energy scales in the two panels.

the localized regime can also be treated within the scattering cross section approach as shown in our previous work.[9]

The vacancy TB model does not directly correspond to a real monovacancy or a hydrogen adsorbate. For comparison we have used also the impurity model of Eq. (2). Figure 4(a) shows the calculated scattering cross sections for a 23-AGNR with one adsorbed hydrogen atom. In this case, the cross section from the impurity Hamiltonian is quite close to that from the vacancy model. The impurity model results in a slight asymmetry and shift with respect to the vacancy model. Thus, the simpler vacancy model seems to give a quite adequate scattering cross section for the adsorbed hydrogen.

The great advantage of the scattering cross section formalism is that it makes possible to study scattering in a fully *ab initio* manner, based directly on DFT transport calculations. However, dealing with graphene nanoribbons still requires a remarkable amount of computational time because all the different adsorbate locations across the ribbon need to be solved self-consistently including the lattice relaxation prior to the transport calculation. Moreover, the separate DFT calculations are limited to rather small ribbons, typically below 5 nm in width. We can, however, significantly lower the computational cost by studying the scattering cross sections of bulk systems, that is, systems with periodic boundary conditions perpendicular to the transport direction.

Figure 4(b) shows the scattering cross section for a hydrogen atom on a 23-AGNR calculated both within the DFT and TB schemes. The quite close correspondence indicates that the simple TB model is quite suitable for simple adsorbates, such as hydrogen, that bind on top of a carbon atom. The cross section for a hydrogen atom in bulk graphene, obtained by imposing periodic boundary conditions as described above, is also shown. In the bulk geometry, the van Hove singularities are smoothed out and the central peak is correspondingly broadened. The same considerations thus apply here as for the vacancy hydrogen model discussion relating to Fig. 3: A good qualitative understanding is possible based on a bulk DFT scattering cross section but some of the details are necessarily lost when translating from the infinite bulk system to a ribbon.

As an example of atop adsorption in which the details of the chemical bonding become important and the vacancy TB model cannot predict the scattering cross section accurately enough, we consider the hydroxyl (OH) group. We perform a DFT bulk calculation for the adsorbed OH and compare the cross section with that for adsorbed hydrogen. Figure 5

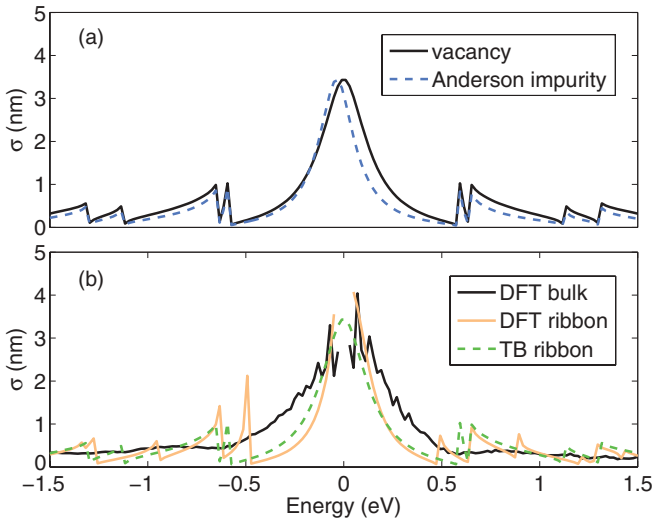

FIG. 4. (Color online) (a) Scattering cross section for a hydrogen atom on a 23-AGNR. The results of the Anderson impurity hydrogen model with $t_A = -2t$ and $e_A = t/16$ and the vacancy model are shown. (b) Scattering cross section for a hydrogen atom on a bulk geometry from DFT and a 23-AGNR calculated with both the DFT and TB models.

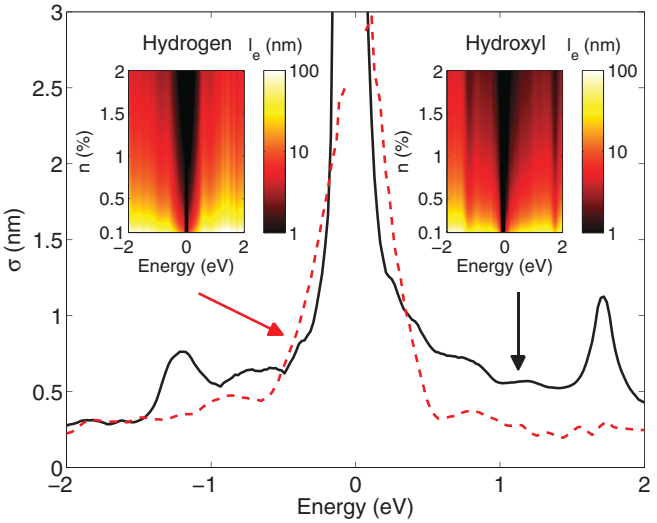

FIG. 5. (Color online) Scattering cross section for a hydrogen atom (dashed line) and a hydroxyl group (solid line) adsorbed on the bulk graphene calculated with DFT. The insets show the corresponding elastic mean free paths for different adatom densities. The scales of the insets have been cut at 1 and 100 nm.

shows that although both adsorbates create a prominent resonance close to the Dirac point, hydroxyl adsorption results in a more asymmetric central peak and additional smaller resonances farther away from the Dirac point. These features serve as the distinguishable fingerprints between hydrogen and hydroxyl. This shows the usefulness of the scattering cross section as a scattering fingerprint, the bulk cross section especially depends only on the adsorbate species and has a characteristic shape for each adsorbate. The insets in Fig. 5 show the estimated elastic mean free paths for the hydrogen and hydroxyl adsorbates, based on the single-defect cross sections. Even small concentrations of such adsorbates lead to very short mean free paths close to the Dirac point, and the effects of the side peaks in the scattering cross section can also be clearly seen.

IV. BRIDGE ADSORBATES: EPOXIDE AND CARBON ADATOM

We now turn to the more complicated case of bridge-bonded adsorbates. As previously, when defect-defect interactions are negligible, a single-defect DFT calculation may be used to estimate the mean free path of a large-scale system. However, with large concentrations of defects, the scatterers start to interact, and to capture these effects large-scale calculations are needed. These are most conveniently done using the TB method, which is able to simulate systems with large numbers of adsorbates. The TB model parameters can be optimized against the corresponding DFT-based single-defect scattering cross section. Here we present optimized TB parameters for epoxide and carbon adsorbates.

Oxygen preferably binds to graphene on the bridge site between carbon atoms and forms an epoxide group. Figure 6 shows the scattering cross section calculated for epoxide on bulk graphene. Unlike the case of hydrogen, there are now three different bridge sites with respect to electron current direction and one needs to average the scattering cross section over them. The most prominent feature of the

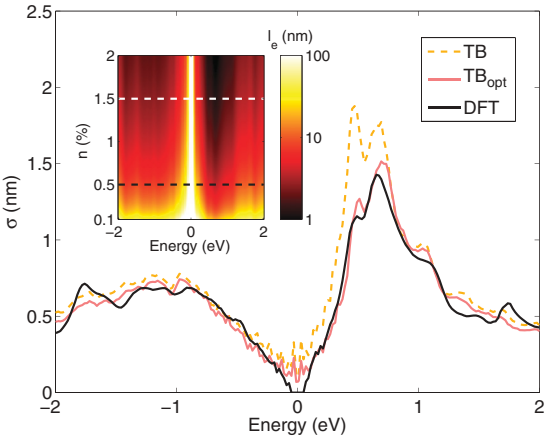

FIG. 6. (Color online) Scattering cross section for an oxygen adatom on bulk graphene (epoxide) averaged over the three different bridge sites. The results of DFT and two TB approaches with different parameter sets are shown. The inset shows the elastic mean free path for different adsorbate concentrations. The scale of the inset has been cut at 1 and 100 nm.

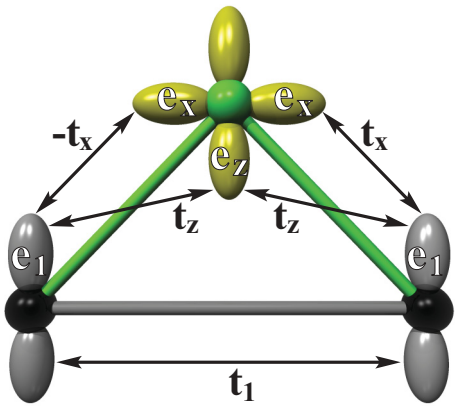

FIG. 7. (Color online) Tight-binding hopping terms t between the two states of the bridge adatom (top) and the two carbon atoms on the graphene plane. The state energies e are also shown.

scattering cross section is the peak above the Fermi energy, corresponding to the oxygen acceptor state in the density of states. This quasilocalized state couples with the electronic states of graphene causing increased scattering for electrons as compared to holes. This is also reproduced by two different sets of TB results, also presented in Fig. 6. The yellow (light gray) curve has been obtained by using the parameters from Ref. 35, but the agreement between TB and DFT can be improved by optimizing the parameters to better match the scattering cross section. The optimized parameter set is $e_1 = -3.79$ eV, $e_x = -2.78$ eV, $e_z = 0.04$ eV, $t_1 = -1.15\,t$, $t_z = -1.22\,t$, and $t_x = 2.50\,t$ (for notation, see Fig. 7). In agreement with Ref. 35, we have used $t = -2.6$ eV. The resulting cross section is shown by the red (dark gray) curve in Fig. 6. As can be seen, the main resonance is captured more accurately by the optimized model. However, additional small resonances close to ± 2 eV are not reproduced. These are better seen in the inset, which

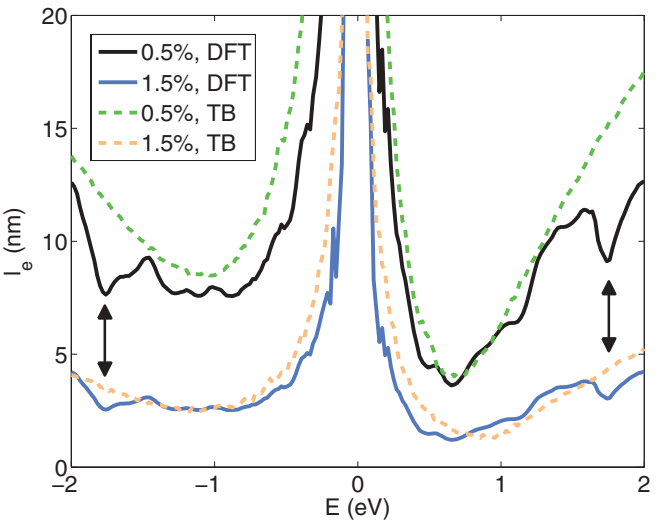

FIG. 8. (Color online) Mean free paths for epoxide adsorbates at two different concentrations. DFT estimates based on single-defect systems are shown with solid lines, while ensemble-averaged TB results for large-scale many-defect systems are shown with dashed lines. The arrows indicate resonances not captured by the TB model.

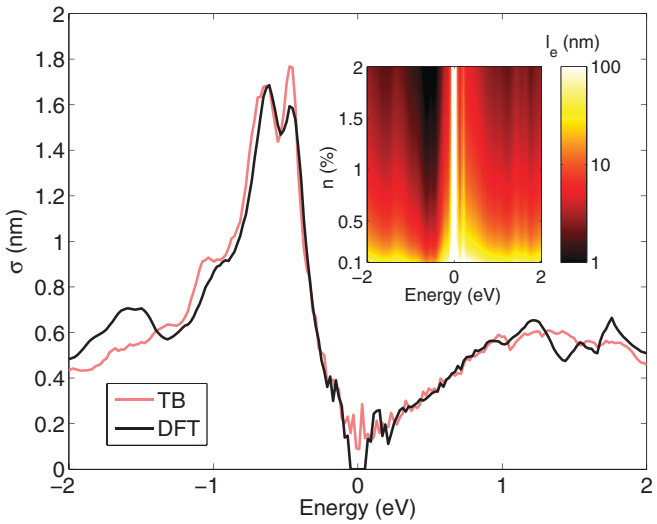

FIG. 9. (Color online) Scattering cross section for a carbon adatom on bulk graphene. The inset shows the elastic mean free path as a function of adatom concentration. The scale of the inset has been cut at 1 and 100 nm.

shows the DFT-based elastic mean free path l_e for different concentrations of epoxide adsorbates. Away from the Dirac point, the most prominent feature is located roughly at 0.6 eV, where the resonance produces a clear drop in l_e. This agrees very well with Kubo-Greenwood calculations.[12,13]

The DFT estimates of l_e are directly based on the scattering cross section of Fig. 6 and the use of Eq. (5). To test the validity of this procedure, we have performed large-scale TB simulations of systems with defect concentrations of 0.5% and 1.5% (these values correspond to the dashed lines in the inset of Fig. 6), by ensemble averaging the results over different configurations of adsorbate locations. The calculations have been performed using a 12 nm × 32 nm unit cell and an ensemble size of 50. Results obtained through this procedure are compared with DFT predictions in Fig. 8. In general, the results agree fairly well, indicating that the transport properties of a large-scale system with a moderate concentration of adsorbates can be reliably estimated based on only a single-defect calculation. No intermediate steps are needed for this procedure, and DFT can thus be directly used to calculate various transport-related properties.

Carbon binds to graphene, like oxygen, on the carbon-carbon bridge.[36,37] The electronic properties of the carbon adsorbate are quite different from those of the epoxide adsorbate, which is reflected in the clearly different scattering cross sections. Indeed, Fig. 9 shows that the characteristic scattering fingerprint in the bulk scattering cross section mirrors intriguingly the epoxide case with a peak below the Fermi level. This feature is a direct result of the sp^3 bond below the Fermi level. We are not aware of previous TB parameters for the carbon adsorbate, so we have optimized the same set of parameters as used above for epoxide[35] by matching the scattering cross sections. The optimized parameters, using the same notation as in the oxygen case, are $e_1 = -4.00$ eV, $e_x = 0.82$ eV, $e_z = 3.85$ eV, $t_1 = -0.13\,t$, $t_z = 1.87\,t$, and $t_x = 1.30\,t$. Here we again use $t = -2.6$ eV. As can be seen in Fig. 9, by using these parameters the TB result matches very well with the DFT-based cross section, apart from minor differences at large energies. As in the case of epoxide, the elastic mean free path shows a clear asymmetry between positive and negative energies. Furthermore, it is important to note that both bridge adsorbates scatter charge carriers mainly at finite energies, whereas the atop adsorbates cause very strong scattering close to the Dirac point.

V. SUMMARY AND CONCLUSIONS

The scaling approach using defect-specific energy dependent scattering cross sections enables the modeling of electronic transport properties of device-scale graphene systems with homogeneous defect distributions. The idea is that the scattering cross section can be determined on the basis of an electron transport calculation for a finite system containing a single defect. In this work we have studied the sensitivity of determining the cross section on the different electronic structure methods (DFT and TB) and different system geometries (bulk graphene and graphene nanoribbons). We have found that a carefully constructed TB model works well for various different adsorbates. Furthermore, the scattering cross section is an useful quantity in validating the TB model, and can even be used to optimize the model parameters, as we have shown above for the case of the bridge-carbon.

The scattering cross section provides a fingerprint which can be used to categorize and compare different defects, especially adsorbate species. An adsorbed hydrogen causes a strong peak in the cross section at the Fermi level and the hydroxyl group exhibits also less intense but clear peaks below and above the Fermi level. Both the hydrogen and hydroxyl adsorb on top of a carbon atom. Oxygen in the form of epoxide and carbon adatoms bind to two carbon atoms at the bridge position. In the case of epoxide the scattering cross section indicates that electrons are scattered more readily than holes, while for carbon adatoms the opposite is true.

ACKNOWLEDGMENTS

This research has been supported by the Academy of Finland through its Centers of Excellence Program (Project No. 251748). Computational resources were provided by CSC–IT Center for Science Ltd. and the Aalto Science-IT project.

*karri.saloriutta@aalto.fi

[1] A. H. Castro Neto, F. Guinea, N. M. R. Peres, K. S. Novoselov, and A. K. Geim, Rev. Mod. Phys. **81**, 109 (2009).
[2] S. Das Sarma, S. Adam, E. Hwang, and E. Rossi, Rev. Mod. Phys. **83**, 407 (2011).
[3] Y. Zhang, V. W. Brar, C. Girit, A. Zettl, and M. F. Crommie, Nat. Phys. **5**, 722 (2009).
[4] S. Adam, E. H. Hwang, V. M. Galitski, and S. Das Sarma, Proc. Natl. Acad. Sci. USA **104**, 18392 (2007).

[5]F. Giannazzo, S. Sonde, R. Lo Nigro, E. Rimini, and V. Raineri, Nano Lett. **11**, 4612 (2011).
[6]A. Ferreira, J. Viana-Gomes, J. Nilsson, E. R. Mucciolo, N. M. R. Peres, and A. H. Castro Neto, Phys. Rev. B **83**, 165402 (2011).
[7]T. Markussen, R. Rurali, A.-P. Jauho, and M. Brandbyge, Phys. Rev. Lett. **99**, 076803 (2007).
[8]T. Markussen, R. Rurali, X. Cartoixà, A.-P. Jauho, and M. Brandbyge, Phys. Rev. B **81**, 125307 (2010).
[9]A. Uppstu, K. Saloriutta, A. Harju, M. Puska, and A.-P. Jauho, Phys. Rev. B **85**, 041401 (2012).
[10]T. O. Wehling, S. Yuan, A. I. Lichtenstein, A. K. Geim, and M. I. Katsnelson, Phys. Rev. Lett. **105**, 056802 (2010).
[11]J. P. Robinson, H. Schomerus, L. Oroszlány, and V. I. Fal'ko, Phys. Rev. Lett. **101**, 196803 (2008).
[12]N. Leconte, A. Lherbier, F. Varchon, P. Ordejon, S. Roche, and J.-C. Charlier, Phys. Rev. B **84**, 235420 (2011).
[13]A. Cresti, A. López-Bezanilla, P. Ordejon, and S. Roche, ACS Nano **5**, 9271 (2011).
[14]J. O. Sofo, A. S. Chaudhari, and G. D. Barber, Phys. Rev. B **75**, 153401 (2007).
[15]D. C. Elias, R. R. Nair, T. M. G. Mohiuddin, S. V. Morozov, P. Blake, M. P. Halsall, A. C. Ferrari, D. W. Boukhvalov, M. I. Katsnelson, A. K. Geim, and K. S. Novoselov, Science **323**, 610 (2009).
[16]A. Bostwick, J. L. McChesney, K. V. Emtsev, T. Seyller, K. Horn, S. D. Kevan, and E. Rotenberg, Phys. Rev. Lett. **103**, 056404 (2009).
[17]Z. Xu and K. Xue, Nanotechnology **21**, 45704 (2010).
[18]T. Sun and S. Fabris, Nano Lett. **12**, 17 (2012).
[19]D. W. Boukhvalov and M. I. Katsnelson, J. Am. Chem. Soc. **130**, 10697 (2008).
[20]J.-A. Yan, L. Xian, and M. Y. Chou, Phys. Rev. Lett. **103**, 086802 (2009).
[21]S. Park and R. S. Ruoff, Nat. Nanotechnol. **4**, 217 (2009).
[22]G. Lu, L. E. Ocola, and J. Chen, Nat. Nanotechnol. **94**, 83111 (2009).
[23]F. Banhart, J. Kotakoski, and A. V. Krasheninnikov, ACS Nano **5**, 26 (2011).
[24]H. Haug and A.-P. Jauho, *Quantum Kinetics in Transport and Optics of Semiconductors*, 2nd ed., Springer Series in Solid State Sciences, Vol. 123 (Springer, Berlin, 2008).
[25]J. M. Soler, E. Artacho, J. D. Gale, A. García, J. Junquera, P. Ordejón, and D. Sánchez-Portal, J. Phys.: Condens. Matter **14**, 2745 (2002).
[26]M. Brandbyge, J.-L. Mozos, P. Ordejón, J. Taylor, and K. Stokbro, Phys. Rev. B **65**, 165401 (2002).
[27]S. Yuan, H. De Raedt, and M. I. Katsnelson, Phys. Rev. B **82**, 115448 (2010).
[28]J. P. Perdew, K. Burke, and M. Ernzerhof, Phys. Rev. Lett. **77**, 3865 (1996).
[29]Q. Li, E. H. Hwang, E. Rossi, and S. Das Sarma, Phys. Rev. Lett. **107**, 156601 (2011).
[30]D. Soriano, N. Leconte, P. Ordejón, J.-C. Charlier, J.-J. Palacios, and S. Roche, Phys. Rev. Lett. **107**, 016602 (2011).
[31]N. Leconte, D. Soriano, S. Roche, P. Ordejon, J.-C. Charlier, and J. J. Palacios, ACS Nano **5**, 3987 (2011).
[32]O. V. Yazyev and L. Helm, Phys. Rev. B **75**, 125408 (2007).
[33]I. Deretzis, G. Fiori, G. Iannaccone, and A. La Magna, Phys. Rev. B **81**, 085427 (2010).
[34]D. H. Choe, J. Bang, and K. J. Chang, New J. Phys. **12**, 125005 (2010).
[35]N. Leconte, J. Moser, P. Ordejón, H. Tao, A. Lherbier, A. Bachtold, F. Alsina, C. M. Sotomayor Torres, J.-C. Charlier, and S. Roche, ACS Nano **4**, 4033 (2010).
[36]P. O. Lehtinen, A. S. Foster, Y. Ma, A. V. Krasheninnikov, and R. M. Nieminen, Phys. Rev. Lett. **93**, 187202 (2004).
[37]K. Nordlund, J. Keinonen, and T. Mattila, Phys. Rev. Lett. **77**, 699 (1996).